Journal of Materials Research and Technology 29 (2024) 2448–2457

Contents lists available at ScienceDirect

Journal of Materials Research and Technology

journal homepage: www.elsevier.com/locate/jmrt

Effects of aging state on the low-cycle fatigue properties of 2024 aluminum alloy

B.S. Gong [a], Z.J. Zhang [a,*], J.P. Hou [a], R. Liu [a], Q.Q. Duan [a], H.W. Wang [a], X.G. Wang [a], H.Z. Liu [a], H. Wang [b], G. Purcek [c], M. Demirtas [d], H. Yanar [c], Z.F. Zhang [a,**]

[a] Institute of Metal Research, Chinese Academy of Sciences, Shenyang, 110016, China
[b] Shenyang Institute of Automation Chinese Academy of Sciences, 110000, China
[c] Department of Mechanical Engineering, Karadeniz Technical University, Trabzon, 61080, Turkey
[d] Department of Mechanical Engineering, Recep Tayyip Erdogan University, Rize, 53100, Turkey

ARTICLE INFO

Keywords:
2024 Al alloy
Aging state
Low-cycle fatigue
Fatigue life
Hysteresis energy
Dislocation slip mode

ABSTRACT

To reveal the effects of aging state on the low-cycle fatigue (LCF) performance of 2024 Al alloy, LCF experiments were conducted on the 2024 Al alloy with three aging states (underaged (UA), peak-aging (PA) and overaged (OA)), respectively. It is found that under the total strain amplitude and plastic strain amplitude control, the Al alloy at UA and OA states exhibits higher LCF lives than that at PA state, respectively. For a more comprehensive evaluation, a hysteretic energy model with W_0 as the fatigue damage capacity and β as the fatigue damage resisting exponent was used, which also shows the advantages of the OA states. This is because although the OA state has lower fatigue damage capacity W_0 for the inferior strength-plasticity combination compared to the UA state, it has higher fatigue damage resistance exponent β because the obvious wavy slip manner of dislocations is conducive to strain homogenization, which is more important for increasing the fatigue life. Therefore, this study gives a comprehensive evaluation and revelation on the effects of aging state on the LCF properties of 2024 alloy.

1. Introduction

With the rapid development of industrialization, the design concepts of engineering materials pay more and more attention to fatigue performance. High-strength Al alloys are often subjected to high loads during service. At this point, the material or component is subjected to alternating stresses that sometimes exceed its yield strength, leading to plastic deformation and failure [1,2]. As a typical representative of high-strength Al alloy, 2024 Al alloy is widely used in aircraft skins, wings, truss beams, landing gear and other key components [3–5]. It is estimated that fatigue-induced failure of engineering components accounts for more than 80 % of all failures [6,7]. Therefore, an in-depth study of the fatigue behavior of wrought Al alloys in the range of large strain/stress amplitude is of great scientific and engineering significance.

Precipitation strengthening has attracted much attention as an important strengthening mechanism affecting the microstructure and fatigue behavior of Al alloys [8–19]. The effect of dislocation slip mode on the fatigue properties of Al alloys under different loading mode conditions is significantly different. For fatigue crack propagation (FCP) behavior, the underaged (UA) state with slip planarity is usually considered to exhibit optimal FCP resistance [9–13]. Additionally, our previous research on the high-cycle fatigue (HCF) performance of wrought Al alloys showed that the overaged (OA) state with cross-slip dislocations shows optimal fatigue properties for high-strength Al alloys (2024 and 7075); however, for medium-strength Al alloys (6A01), the peak-aging (PA) state exhibits the highest fatigue strength, which is attributed to its higher tensile strength increasing the alloy's deformation resistance [14,15]. For low-cycle fatigue (LCF) of Al alloys, there is a general concern about cyclic response behavior, and UA alloys usually exhibit cyclic hardening characteristics due to dynamic precipitation during cyclic loading [16–19]. However, little has been reported about the effect of aging time on LCF life.

Based on the LCF life prediction Coffin-Manson relationship [20,21]:

$$\varepsilon_p = \varepsilon_f (2N_f)^c, \tag{1}$$

* Corresponding author.
** Corresponding author.
E-mail addresses: zjzhang@imr.ac.cn (Z.J. Zhang), zhfzhang@imr.ac.cn (Z.F. Zhang).

https://doi.org/10.1016/j.jmrt.2024.01.212
Received 30 October 2023; Received in revised form 10 January 2024; Accepted 23 January 2024
Available online 5 February 2024

where: ε_p-plastic strain, ε_f-fatigue ductility factor, N_f-fatigue life, c-fatigue ductility exponent, it is generally believed that materials with excellent plasticity are generally considered to exhibit good LCF performance. For example, Mughrabi et al. [22–24] investigated the fatigue behavior of ultrafine and coarse crystalline materials. The results showed that ultrafine crystalline with high strength exhibited excellent HCF properties, while coarse crystalline materials with good tensile plasticity exhibited excellent LCF properties.

Furthermore, compared to cross-slip, planar slip has a positive effect on delaying crack initiation and eventual fatigue failure due to excellent deformation reversibility [25]. For example, previous studies have shown that the stacking fault energy (SFE) of Cu–Al alloys decreases as the Al content increases, which effectively increases the slip planarity of the alloy, leading to an increase in both HCF and LCF lives [26–28]. However, Shao et al. [29] studied the cyclic deformation and damage behavior of Fe–Mn and Fe–Mn–C TRIP/TWIP steels and found that the dislocation structure transformed from cross-slip to planar slip after cyclic deformation as the C content increased (an increase of short-range ordering (SRO)), but the LCF performance became worse instead. The reason for the inconsistency between the results of the above two experiments is that the deformation uniformity caused by decreasing the SFE and increasing the SRO is different. Considering the nature of the SFE, the planar slip due to the reduction of the SFE is uniformly distributed, which increases the degree of deformation homogenization. As a result, the material exhibits little fatigue damage. However, increasing SRO tends to lead to the accumulation of planar slip in certain dislocation bands, which exacerbates the fatigue damage localization.

To sum up, the excellent plasticity and the planar slip caused by the reduction of the SFE can improve LCF performance of the material. Previous studies have shown that the Al alloy at the UA state exhibits a good strength-plasticity matching relationship compared to the OA state [30–33], which seems to have a positive effect on LCF performance. However, for Al alloys, reducing SFE by aging has very little effect [34]. Therefore, the slip planarity of the UA state should be caused by a mechanism similar to SRO [35–37], which is detrimental to the LCF performance of Al alloy. So, which dominates LCF performance of 2024 Al alloy, the tensile properties or the slip mode? Previous studies [16–19] have more often dealt with the effects of deformation mechanisms or tensile properties on LCF properties of Al alloys individually without considering the coupling factors of the two. Therefore, it is of great engineering and scientific significance for the design of fatigue-resistant Al alloys to reveal the effect of aging state on the LCF properties of Al alloys from the perspectives of both microscopic mechanisms and tensile properties.

The present work focuses on the LCF behavior of 2024 Al alloy at different aging states. In contrast to previous work that considered only a single factor, this study comprehensively analyzes the effects of plasticity and dislocation slip mode on LCF performance of 2024 Al alloy. Additionally, total strain amplitude $\Delta\varepsilon/2$-fatigue life N_f, plastic strain amplitude $\Delta\varepsilon_p/2$-fatigue life N_f and hysteretic energy W_a-fatigue life N_f relationship curves were established, which are effective for guiding the fatigue-resistant design of Al alloys.

2. Experimental procedures

In this work, the material selected is a 2024 Al alloy rolled sheet, supplied by the manufacturer. The specific production process is casting-rolling-annealing-solid solution-deformation-aging. We performed solid-solution + aging treatment on the purchased 2024 Al alloy, the process flow is shown in Fig. 1(a). Based on the aging hardening curves in Figs. 1(b), 180 °C/2 h, 180 °C/16 h and 180 °C/36 h were selected as the UA, PA and OA states of 2024 Al alloy, respectively.

The purpose of selecting UA and OA states with the same hardness or strength is to better reveal the general regularity of the effect of deformation mechanisms on LCF performance of 2024 Al alloy under the same strength level. The chemical composition of 2024 Al alloy was shown in Table 1.

To avoid the deformation of tensile and fatigue specimens of 2024 Al alloy during heat treatment, the required dimensions of tensile and fatigue specimens were first cut from the 2024 Al alloy plate. Then, the solution treatment was carried out in a chamber furnace and quenched in water, quench transfer time of less than 3 s. Finally, they were aged in an electrically heated oil bath and cooled in air. Tensile and fatigue specimens were machined after the heat treatment process was completed. Tensile experiments of 2024 Al alloy were carried out on an Instron 5982 electronic testing machine, with a tensile rate of $10^{-3}s^{-1}$. The cross-sectional area of the tensile specimen is 4 mm × 4 mm, and the length of the working segment is 12 mm. Fig. 2 shows the LCF specimen size of 2024 Al alloy. The LCF test was conducted on 2024 Al alloy using an Instron 8862 testing machine with a frequency of 0.5 Hz and the stress ratio R = −1. It should be noted that tensile and LCF ($\Delta\varepsilon/2$ = 0.4%-$\Delta\varepsilon/2$ = 0.8 %) experiments were performed on two parallel specimens in each aging state.

The grain morphology of 2024 Al alloy at different aging states was observed using BX53 M metallurgical microscope (OM) and Sigma 500 scanning electron microscope (SEM). JSM-6510 SEM was used to observe the surface damage morphologies of 2024 Al alloy at different aging states. The surface distortion degree of the samples after LCF was observed by electron backscatter diffraction (EBSD) technique with a sigma 500 SEM. Transmission Electron Microscopy (TEM) samples of 2024 Al alloy were prepared by a twin-jet polishing method in a solution of HNO_3:CH_3OH = 1:9 (vol.), working voltage 15 V, temperature −25 °C. The matrix precipitated phase morphologies and dislocation

Table 1
Chemical composition (in wt%) of 2024 Al alloy.

Element	Cu	Mg	Zn	Mn	Fe	Si	Al
Content	4.5	1.5	0.25	0.58	0.5	0.5	Bal

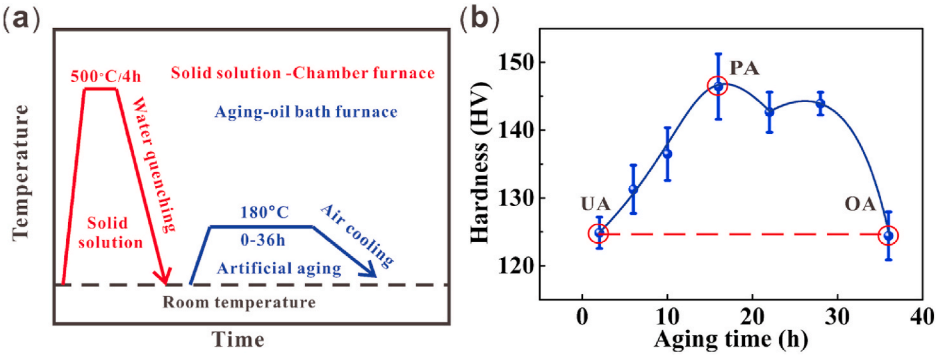

Fig. 1. (a) Schematic diagram of 2024 Al alloy heat treatment process; (b) the change in hardness of 2024 Al alloy with increasing aging time.

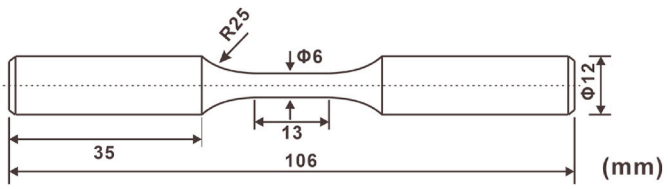

Fig. 2. LCF specimen size of 2024 Al alloy.

evolution forms of 2024 Al alloy was observed by FEI Tecnai F20 TEM.

3. Experimental results

3.1. Microstructure

To investigate the effect of aging state on microstructure of 2024 Al alloy, OM and EBSD observations were carried out on the samples at different aging states. As can be seen from Fig. 3, the grains show a flattened shape in all three aging states. Furthermore, there is no significant change in grain size and grain orientation with increasing aging time, which is usually associated with lower aging temperatures. Based on the OM and EBSD observations, it can be concluded that the effect of aging state on LCF behavior of 2024 Al alloy is independent of grain size and grain orientation. From this, it can be deduced that the main factor affecting the LCF behavior of 2024 Al alloys is the precipitated phase morphology.

Fig. 4 illustrates the precipitated phase structure of 2024 Al alloy under TEM. Based on the previous study [38,39], the precipitation sequence of 2024 Al alloy is SSS → GP (I, II) zones → S″ → S′ → S (Al_2CuMg), where SSS is a supersaturated solid solution. As a result, the UA state precipitated GP zones coherent with the matrix and distributed in clusters, as shown in Fig. 4(a). With increasing aging time, the GP zone growth and coarsening, forming S′ and S phases that are semi-coherent and incoherent with the matrix at the PA and OA states, respectively (Fig. 4(b) and (c)).

3.2. Tensile properties

Based on the previous study [14], Fig. 5(a) shows the tensile curves for the three aging states. The aging state samples exhibit higher strength compared to the solid solution state. Besides, the UA state shows lower yield strength but higher tensile strength compared to the OA state, which indicates that the UA state has better work-hardening ability. From the strength-plasticity relationship in Fig. 5(b), the PA state has the highest tensile strength and the UA state has the best strength-plasticity match among the three aging states. The tensile properties of 2024 Al alloy at different aging states are consistent with the previous studies [30,40,41].

3.3. Cyclic stress response behavior

From Fig. 6(a)-6(c), it can be seen that the cyclic stress response behavior of 2024 Al alloy at three aging states shows significant differences. Both the UA and PA states exhibit cyclic hardening characteristics, while the cyclic hardening ability of PA state is weaker than that of UA state. For the OA state, it shows cyclic softening at high-strain amplitudes ($\Delta\varepsilon/2 = 0.6\%$-$\Delta\varepsilon/2 = 0.8\ \%$) but first hardening followed by softening at low-strain amplitudes ($\Delta\varepsilon/2 = 0.4\ \%$ and $\Delta\varepsilon/2 = 0.5\ \%$). Based on previous studies [42], the cyclic softening behavior exhibited of the OA state at higher strain amplitudes is due to dislocations cutting through the precipitated phases of the partially coherent. However, as the strain amplitude decreases, a small number of dislocations preferentially accumulate inside the matrix during the early stages of plastic deformation, thus exhibiting a cyclic hardening behavior. As the number of cycles increases, dislocations increase and cut through the second phase, thus exhibiting cyclic softening.

To visually reflect the cyclic stress response behavior of the three aging states, Fig. 6(d) summarizes the saturation stress amplitudes at different strain amplitudes. The saturation stress amplitudes of 2024 Al alloy at the three aging states show a monotonic increasing trend with the increase of the strain amplitude. The UA state exhibits the highest saturation stress compared to the PA and OA states for the same strain amplitude.

3.4. Hysteresis loop curves

Fig. 7 illustrates the stress-strain hysteresis loop curve of the half-life data. The results show that both the shape and area show significant differences. The hysteresis loop curve is similar to the spindly shape at the UA state, while the OA state exhibits a chubby. Furthermore, the hysteresis loop area is larger for the OA state than that of the UA state, which indicates that the OA alloy absorbs more external work during plastic deformation [43]. However, whether all of the absorbed external workings are converted into effective damage is closely related to the mode of dislocation slip, which is described in more detail later in the discussion section.

3.5. Fatigue properties

The total strain amplitude $\Delta\varepsilon/2$ and the fatigue life N_f curves for the

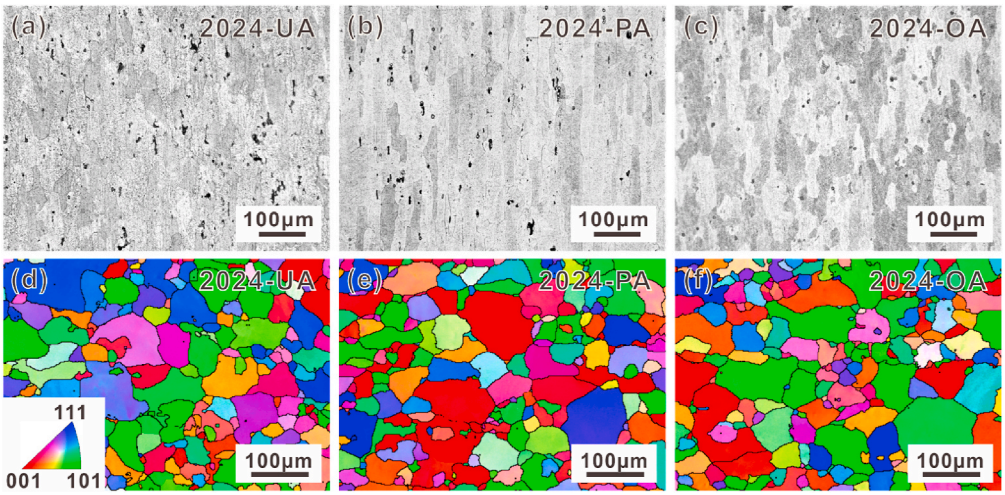

Fig. 3. Grain morphology of 2024 Al alloy at different aging states. (a) and (d) UA; (b) and (e) PA; (c) and (f) OA.

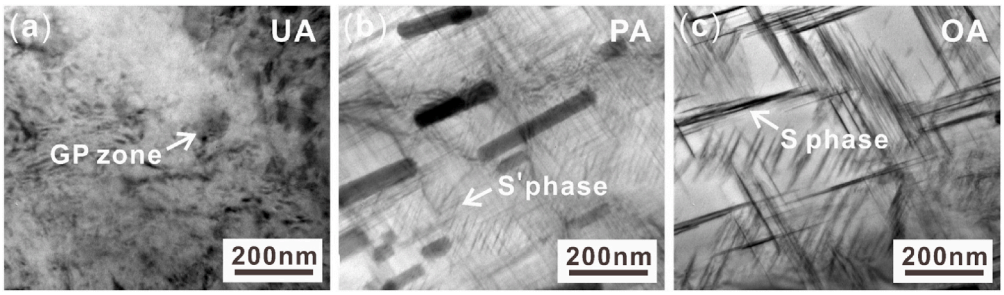

Fig. 4. The matrix precipitated phases morphologies of the (a) UA, (b) PA and (c) OA states of 2024 Al alloy, respectively.

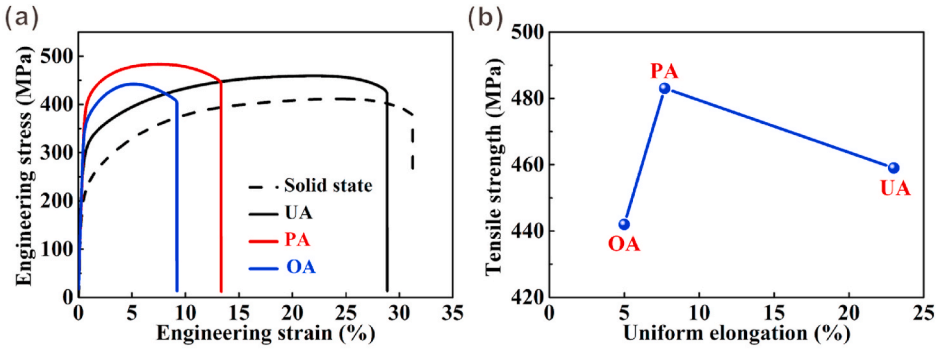

Fig. 5. Results of tensile properties of 2024 Al alloys in three aging states. (a) engineering stress-strain curves; (b) tensile strength and uniform elongation relationship.

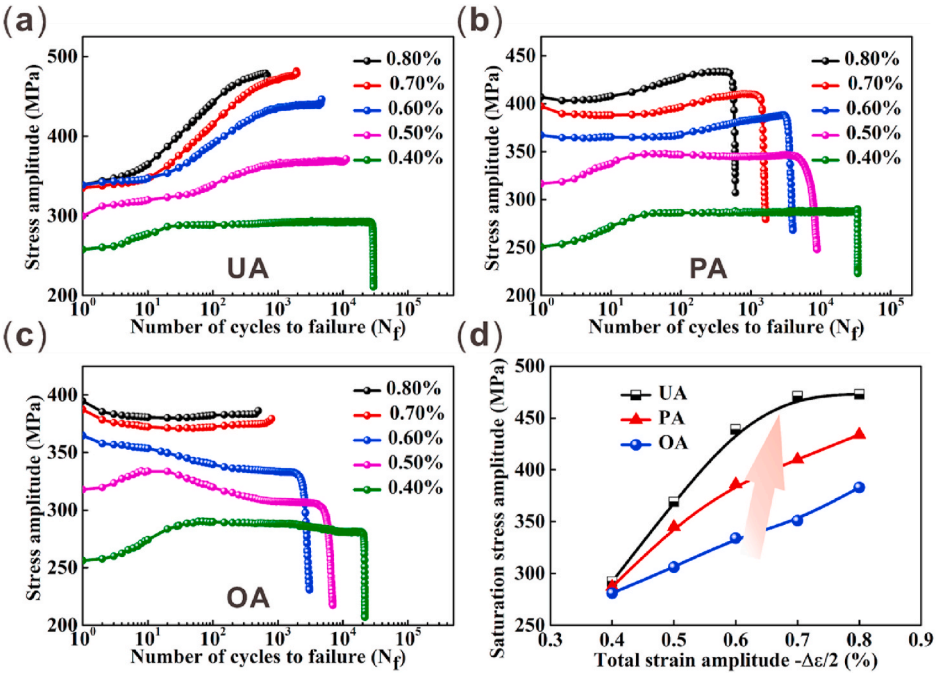

Fig. 6. (a)–(c) Cyclic stress response behaviors of 2024 Al alloys at different aging states; (a) UA; (b) PA; (c) OA; (d) trend of saturation stress amplitude with increasing strain amplitude.

three aging states are shown in Fig. 8(a). It can be seen that the $\Delta\varepsilon/2-N_f$ curves for the UA and OA states are almost parallel. The slopes and intercepts of $\Delta\varepsilon/2-N_f$ curves for the UA, PA and OA states are −0.18, −0.17 and −0.19; 0.41, 0.36 and 0.41, respectively. The fatigue life of the UA state is slightly higher than that of the PA and OA states at the same strain amplitude. Previous researchers have also found results consistent with ours in studies of LCF properties of 6063 Al alloys [44]. It has been shown that strain-induced vacancy-driven dynamic precipitation leads to dramatic cyclic hardening of UA alloys resulting in improved fatigue life. However, the results of the plastic strain amplitude $\Delta\varepsilon_p/2$ and fatigue life N_f curves of the half-life data show that have excellent fatigue properties of the OA alloy at the same strain amplitude, as shown in Fig. 8(b). The slopes and intercepts of the $\Delta\varepsilon_p/2$- N_f curves for the three aging states are −1.76, −1.41, −0.82; 4.52, 3.77, 2.06,

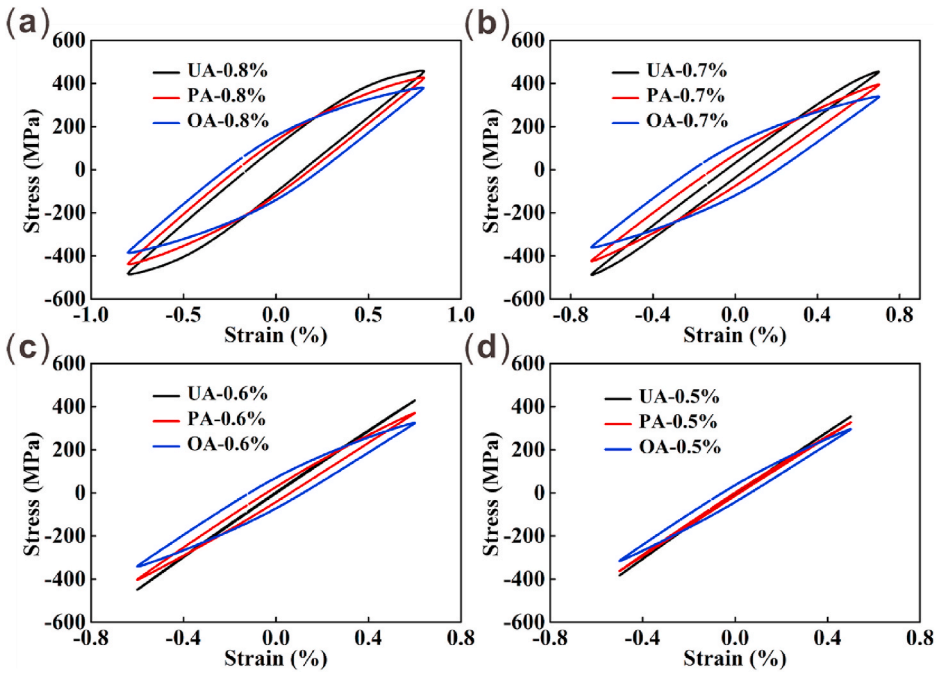

Fig. 7. Stress-strain hysteresis loops for three aging states of 2024 Al alloy at different strain amplitudes. (a) $\Delta\varepsilon/2 = 0.8$ %; (b) $\Delta\varepsilon/2 = 0.7$ %; (c) $\Delta\varepsilon/2 = 0.6$ %; (d) $\Delta\varepsilon/2 = 0.5$ %.

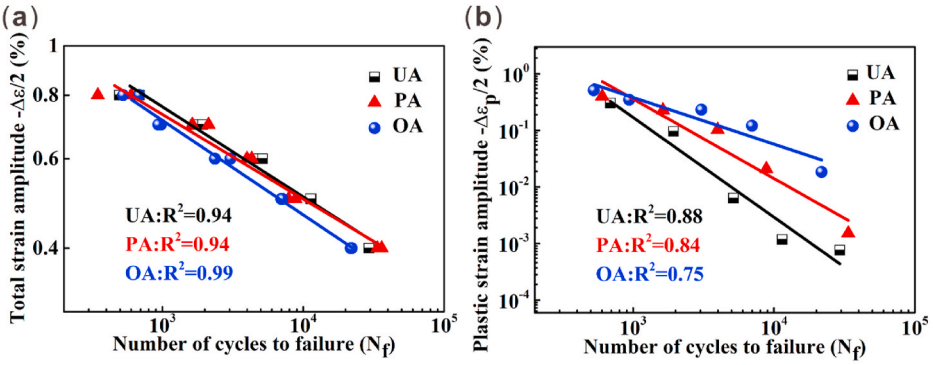

Fig. 8. (a) Total strain amplitude $\Delta\varepsilon/2$-fatigue life N_f curves Δ; (b) plastic strain amplitude $\Delta\varepsilon_p/2$ −fatigue life N_f curves.

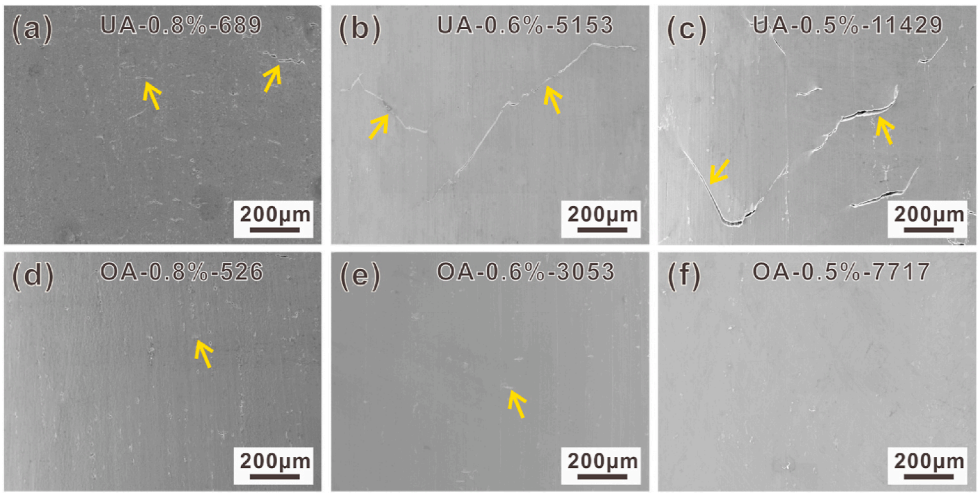

Fig. 9. Surface damage morphologies of the 2024 Al alloy samples at different aging states after the LCF test. (a)–(c) UA; (d)–(f) OA.

respectively. Han et al. [16] also found in their study of Al–Cu alloys that OA alloys exhibit excellent LCF properties at low plastic strain amplitudes. Combined with the results of the previous studies [16,44], it can be tentatively concluded that the UA and OA alloys exhibit excellent fatigue properties under the evaluation criteria of total strain amplitude and plastic strain amplitude, respectively.

3.6. Surface damage morphologies

The surface states of the UA and OA alloys after LCF are shown in Fig. 9. As can be seen in Fig. 9(a)-9(c), several cracks on the surface of the UA alloy indicate that the alloy bears severe strain localization. Unlike the UA sample, only a few microcracks appear on the surface of the OA sample, exhibiting weak fatigue damage and good strain uniformity. The differences in surface damage morphologies of the UA and OA alloys should be related to their saturation stress amplitude. As can be seen in Fig. 6(d), the saturation stress amplitude at the UA state is significantly higher than that of the OA state, which accelerates the fatigue cracking of 2024 Al alloy.

To further illustrate the degree of plastic deformation of 2024 Al alloy at different aging states, the kernel average misorientation (KAM) for both UA and OA samples was observed. Considering that the uneven deformation near the fatigue fracture would affect the accuracy of the experimental results, the ESSD samples were selected at a uniform deformation approximately 3 mm away from the fatigue fracture. The KAM maps and corresponding distributions for the UA and OA samples at $\Delta\varepsilon/2 = 0.6$ % and $\Delta\varepsilon/2 = 0.4$ % strain amplitudes are shown in Fig. 10.

From Fig. 10(a), (b), 10(d) and 10(e), it can be seen that the degree of distortion is more drastic in the UA samples than that of the OA one. Furthermore, as can be seen in Fig. 10(c) and (f), the KAM values are larger for the UA state than for the OA state, both for the average KAM (marked by the dashed line) and for the high KAM region where fatigue cracking is more likely to occur (marked by the red dashed box). In summary, the results of the KAM maps are consistent with the surface crack morphologies regularly, which further indicates that the UA sample exhibits higher strain localization during cyclic loading.

3.7. Dislocation configuration after LCF

The dislocation slip mode during plastic deformation of 2024 Al alloy at different aging states can be reflected by the dislocation structure. Fig. 11 shows the form of dislocation evolution after LCF for samples at different aging states. For the UA sample, a large number of dislocations are uniformly distributed in the matrix, exhibiting a planar slip characterization, as shown in Fig. 11(a). This should be the main reason why the UA state exhibits cyclic hardening behavior. For the PA state (Fig. 11 (b)), some dislocations are located inside the matrix, while others are annihilated and aggregated on the second phase boundary. This form of distribution of dislocations results in a PA state that exhibits weak cyclic hardening. However, for the OA state, the dislocations annihilate and aggregate at the second-phase boundary, accompanied by the emergence of dislocation cells, which exhibit typical wavy slip characteristics, as shown in Fig. 11(c). Dislocation annihilation on the second phase usually leads to cyclic softening of the OA state.

Therefore, the dislocation slip mode changes from a planar slip structure to a cross-slip structure with increasing aging time. For the planar slip mode at the UA state, the dislocation cuts through the second phase and then undergoes long-range slip, so it easily reaches the grain boundaries or sample surface to form a slip band, as shown in Fig. 12(a). The cross-slip dislocations at the OA state are easily annihilated on the second phase boundary, which reduces the number of dislocations reaching the grain boundaries or sample surface. As a result, OA alloys exhibit good deformation uniformity as well as weak fatigue damage, as shown in Fig. 12(b).

4. Analysis and discussion

In scientific research, the HCF life prediction model based on stress control and the LCF life model based on strain control are widely used. For the HCF life prediction model, i.e. the Basquin formula [45] :

$$\sigma_a = \sigma_f \left(2N_f\right)^b , \tag{2}$$

where: σ_a-stress amplitude, σ_f-fatigue strength coefficient, b-fatigue strength exponent. For the LCF life prediction model, i.e., the Coffin-Manson formula [20,21], expressed in Eq [1]. above. Liu et al. [26] developed a hysteretic energy model of fatigue damage by combining the above two fatigue life prediction formulations, which can evaluate the LCF fatigue performance of materials more comprehensively. The hysteresis energy model is as follows:

$$W_a = W_0 \bullet N_f^{-1/\beta} , \tag{3}$$

where W_a is the input hysteresis energy for each cycle, both W_0 and β are material constants. W_0 is defined as the fatigue damage capacity, which represents the ability of a given material to resist fatigue damage, related to the strength-plasticity (toughness) of the material. β is defined as the fatigue damage resisting exponent. Increasing the value of $\boldsymbol{\beta}$

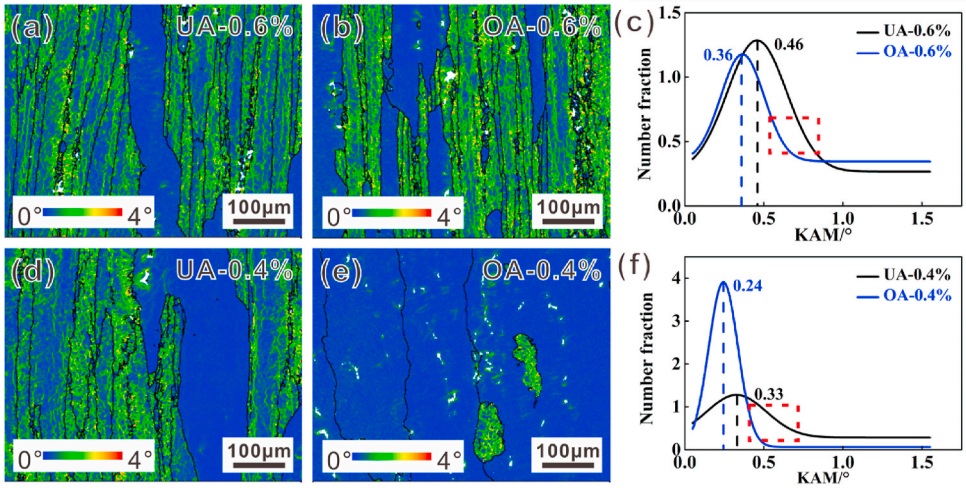

Fig. 10. EBSD results of kernel average misorientation (KAM) maps of 2024 Al alloy. (a) UA-0.6 %; (b) OA-0.6 %; (c) UA-0.4 %; (d) OA-0.4 %, (c) and (f) KAM value distributions of 2024 Al alloy.

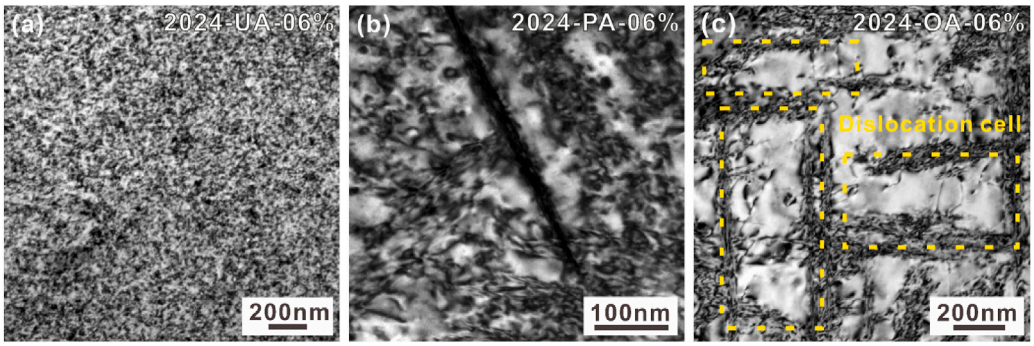

Fig. 11. The dislocation morphologies of 2024 Al alloy in the three aging states at the strain amplitude of 0.6 %. (a) UA; (b) PA; (c) OA.

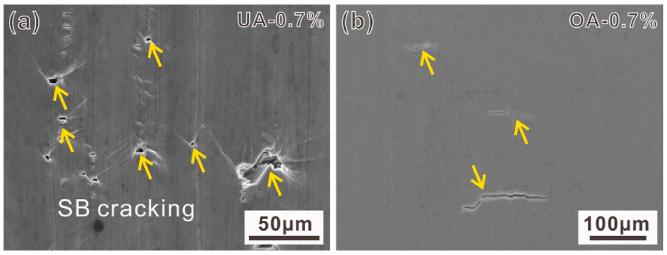

Fig. 12. (a) Micromorphology of the slip bands at the UA samples; (b) distribution condition of fatigue cracks at the OA samples.

means that the conversion rate of the material to effective damage is lower as the external mechanical work accumulates, which slows down the declining rate of fatigue life with the increase of strain amplitude. The increase of both W_0 and β is beneficial to improve the fatigue resistance of the material.

According to Eq. (3), Fig. 13 summarizes the relationship between W_a and N_f of 2024 Al alloy at different aging states. The two constants (W_0 and β) in the energy model can be obtained by least squares fitting. β and W_0 represent the slope and intercept of the W_a-N_f curve, respectively. From the energy point of view, the OA state shows the highest fatigue life when the external work done is consistent. The results of fitting the W_a-N_f and the $\Delta\varepsilon_p/2$ $-N_f$ curves show the same trend.

Fig. 14 shows the change of W_0 and β values of 2024 Al alloy with aging time. The results show that W_0 monotonically decreases and β monotonically increases as the aging time increases. The increase in the β value implies a decrease in the effective fatigue damage transformation rate, which is beneficial to the fatigue performance of the alloy. However, the decrease in the W_0 value represents the reduction in fatigue damage tolerance, which is detrimental to the fatigue

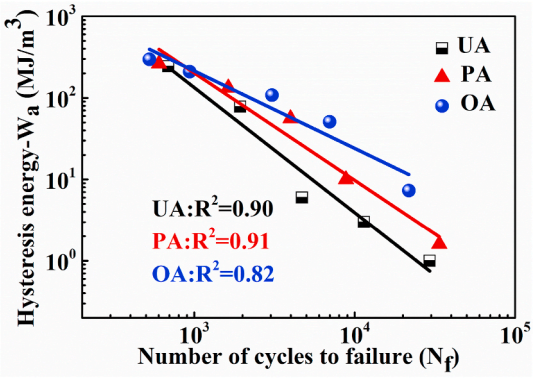

Fig. 13. The relationship between hysteresis loop area *W*a and the fatigue life N_f of 2024 Al alloy at different aging states.

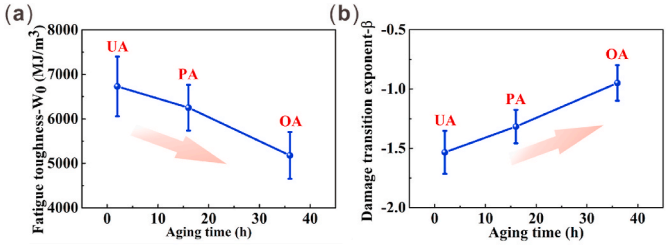

Fig. 14. Relationships between the parameter values of the hysteresis energy model (W_0 and) and the aging times. (a) the regular change in W_0 value; (b) the regular change in β value.

performance of the alloy. As we discussed earlier, W_0 is related to the strength-plasticity of the material, which is influenced by the tensile properties, while the fatigue damage resisting exponent represented by β is mainly related to the deformation mechanism of the material, i.e., the slip modes of dislocation at different aging states. Therefore, the effects of aging state on the LCF properties of 2024 Al alloy from the viewpoint of tensile properties and dislocation slip mode will be analyzed next.

According to the previous study [29], the parameters W_0 and β in the fatigue damage model can be described in the following form：

$$W_0 = 4K \bullet \varepsilon_{t-max} \bullet \sigma_{t-max} \ , \tag{4}$$

$$\beta = -\frac{1}{(1+n')c} \ , \tag{5}$$

where K is the material constant; ε_{t-max} represents the maximum true strain of the true stress-strain curve; σ_{t-max} represents the maximum true stress of the true stress-strain curve. Obviously, $\varepsilon_{t-max} \bullet \sigma_{t-max}$ represents the mechanical energy of the material, similar to the static toughness U of the tensile test. The n' indicates the cycle hardening exponent, which is related to the work hardening capacity of the material. c is the ductility exponent. According to Eq. (4), W_0 is mainly influenced by K and U. Therefore, the following discussion focuses on the effects of K and U values (tensile properties) on the LCF properties of the 2024 Al alloy at different aging states.

Fig. 15(a) shows that W_a in the hysteretic energy model is linearly related to $\Delta\varepsilon_P \bullet \Delta\sigma$. Where $\Delta\varepsilon_P$ represents the plastic strain range, $\Delta\sigma$ represents the corresponding stress range.

$$W_a = K \bullet \Delta\varepsilon_p \bullet \Delta_\sigma . \tag{6}$$

Fig. 15(b) shows what W_a and $\Delta\varepsilon_P \bullet \Delta\sigma$ represent. W_a represents the area of the curve enclosed by the hysteresis loop; $\Delta\varepsilon_P \bullet \Delta\sigma$ value represents the shaded area; K is the shape factor, usually expressed as the ratio of the area enclosed by the hysteresis loop curve to the shaded area. From Fig. 15(c) and (d), it can be seen that the shape factor K and static toughness U values of the 2024 Al alloy show a decreasing trend as the aging time increases. Therefore, based on Eq. (4), the UA samples have

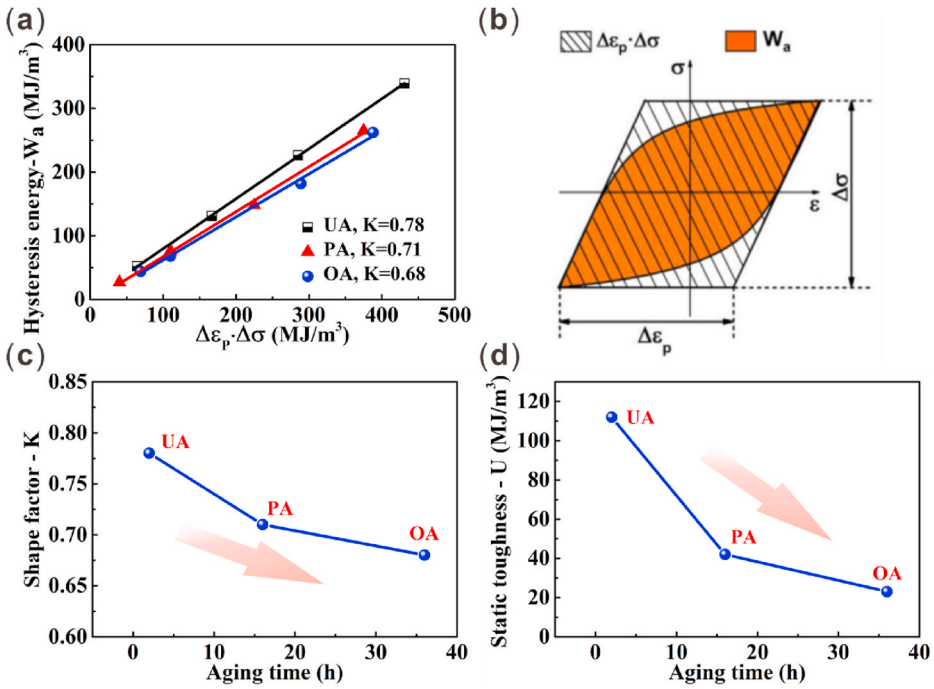

Fig. 15. (a) The relationship between hysteresis loop area W_a and the value of $\Delta\varepsilon_p{\cdot}\Delta\sigma$; (b) explanation of the shape factor K; (c) trend of static toughness with aging time.

the highest fatigue damage tolerance W_0.

Regarding the ductility exponent C in Eq. (5), a mass of experimental results shows that the value of C is constant (≈ -0.6) for metallic materials [46,47]. Therefore, the fatigue damage resisting exponent β is mainly related to the cyclic hardening exponent n'. According to Eq. (5), the larger the value of the material n', the smaller the β. As can be seen from the work-hardening rate curve in Fig. 16, the work-hardening rate reduces as the aging time increases, implying a decrease in hardening capacity. Therefore, the OA state has the largest β value.

Furthermore, based on previous studies [29], the cyclic hardening exponent n' can be calculated by fitting the data with Eq. (7).

$$\frac{\Delta\varepsilon}{2}=\frac{\Delta\sigma}{2E}+\left(\frac{\Delta\sigma}{2k'}\right)^{\frac{1}{n'}} \tag{7}$$

where $\Delta\varepsilon$ is the total strain, $\Delta\sigma$ is the stress, E is the elastic modulus, $\frac{\Delta\sigma}{2E}$ is the elastic strain, k' is the shape factor. The plastic strain expression can be obtained from Eq. (7) as shown in Eq. (8). Taking the logarithm of the left and right sides of Eq. (8), as shown in Eq. (9), it can be seen that $\lg\frac{\Delta\varepsilon_p}{2}$ and $\lg\left(\frac{\Delta\sigma}{2}\right)$ satisfy the linear relationship, where $\frac{1}{n'}$ is the slope and $\lg\frac{1}{k'}$ is the intercept.

$$\frac{\Delta\varepsilon_p}{2}=\left(\frac{\Delta\sigma}{2k'}\right)^{\frac{1}{n'}} \tag{8}$$

$$\lg\frac{\Delta\varepsilon_p}{2}=\frac{1}{n'}\lg\left(\frac{\Delta\sigma}{2}\right)-\lg\frac{1}{k'} \tag{9}$$

Based on Eq. (9), the n' values for the UA and OA states at higher strain amplitudes ($\Delta\varepsilon/2$ = 0.8 %,0.7) were calculated to be −0.39, −0.91; −0.2, −0.58. The above results further demonstrate that the OA state has a higher β value compared to the UA state.

The excellent fatigue damage capacity W_0 of the UA state and the good fatigue damage resisting exponent β of the OA state are closely related to the precipitated phase morphology. For the UA state, the matrix precipitation phase GP zone remains co-lattice with the matrix, so dislocations easily cut the second phase and tend to slip on the same slip surface. In general, planar slip dislocations have a positive effect on the work-hardening capacity and strength-plasticity of the material [34]. Based on these results, it can be seen that the UA state exhibits superior work-hardening rate, strength and elongation compared to the OA state. This is the main reason for the higher fatigue damage capacity of the UA state. However, the OA state precipitates S phase that is incoherent with the matrix as the aging time increases. The incoherent S phase can itself act as a source of dislocation annihilation, which promotes cross slip and annihilation of movable dislocations. As a result, the dislocation ring around the second phase promotes dislocation cross slip and annihilation, which leads to the UA state exhibiting low work-hardening rates, strengths and elongation The OA state has a high fatigue damage resistance exponent because the annihilation of the second phase reduces the number of dislocations reaching the defect and the sample surface.

Based on the analysis above, this work evaluates the LCF performance of 2024 Al alloy in terms of total strain amplitude, plastic strain amplitude and energy model, respectively. Under the evaluation criteria of the total strain amplitude, the fatigue life of the UA state is slightly higher than those of the PA and OA states. However, the OA state exhibits the highest fatigue life based on the evaluation method of plastic strain amplitude and hysteresis energy model. The reason for the

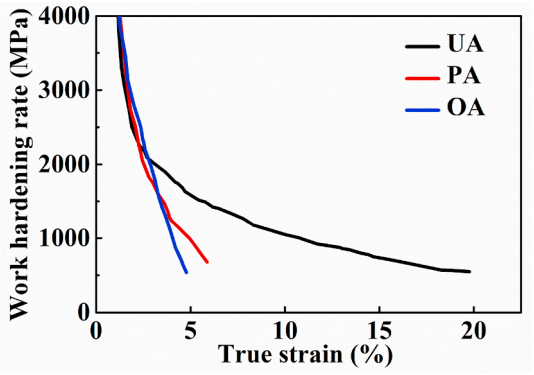

Fig. 16. Work-hardening curve of 2024 Al alloy at different aging states.

inconsistency of the above results is that the dominant factor in the LCF performance of 2024 Al alloy is inconsistent under different evaluation systems. At the total strain amplitude, the LCF properties of Al alloys are more closely related to their tensile properties. The higher fatigue capacity of the UA state improves its resistance to absorbed energy (as shown in Fig. 7), exhibiting higher fatigue life. The LCF properties of 2024 Al alloy are dominated by the dislocation slip mode from the perspective of plastic strain amplitude and energy modeling. The OA alloys absorb more energy during cyclic deformation, but a higher fatigue damage resisting exponent will reduce the energy of effective damage, which plays an important role in improving LCF life. It should be noted that the reason for the high fatigue damage resisting exponent of the OA state is that its wavy dislocations reduce the hardening capacity of the alloy.

In the previous study of Cu–Al alloys, Liu et al. [26] found that the fatigue capacity and fatigue damage resisting exponent of the material increased simultaneously with the increase of Al content. Therefore, whether evaluating the LCF performance of Cu–Al alloys from the viewpoint of total strain amplitude, plastic strain amplitude or energy modeling, the materials with higher Al content exhibit the highest LCF life. In the study of TWIP steel, Shao et al. [29] found that the fatigue capacity increased, but the fatigue damage resisting exponent decreased with increasing C content. The materials with higher C content exhibit the worst LCF properties for all three of these evaluation criteria. For the present study, the UA state with higher fatigue capacity exhibits high LCF life at total strain amplitude. However, the OA state with a high fatigue damage resisting exponent exhibits the best LCF properties when considered in terms of plastic strain amplitude and hysteresis energy model. Combined with the above research, it is better to simultaneously improve the fatigue damage capacity and fatigue damage resisting exponent of materials to obtain better LCF performance. If not, at least the fatigue damage resisting exponent should be improved.

5. Conclusions

This work systematically studies the LCF behavior of 2024 Al alloy, analyzing the changes in fatigue life, cyclic response behavior, surface damage morphology and microstructure evolution regulations. Based on the above experimental results, the following conclusions can be drawn.

1) Based on the fatigue damage hysteresis energy model, the LCF of 2024 Al alloy is determined by the fatigue damage capacity W_0 (related to the tensile properties) and the fatigue damage resistance exponent β (related to the mode of dislocation slip).
2) Under the evaluation criteria of total strain amplitude, the higher fatigue damage capacity W_0 of the UA state contributes to a higher fatigue life. However, the higher fatigue damage resistance exponent β of the OA state gives it excellent fatigue performance under the evaluation criteria of plastic strain amplitude and energy modeling.
3) For cyclic response behavior, planar slip dislocations at the UA state promoted cyclic hardening, while cross-slip dislocations at the OA state led to softening.

Declaration of competing interest

The authors declare that they have no known competing financial interests or personal relationships that could have appeared to influence the work reported in this paper.

Acknowledgements

The authors would like to thank X.H. Zhou, Z.K. Zhao, B. Wang and X.J. Guan for the sample preparation, fatigue tests, SEM, TEM observations and stimulating discussions. This work is financially supported by the National Natural Science Foundation of China (NSFC) under Grant Nos. 52271121, 52322105, 52130002, KC Wong Education Foundation (GJTD-2020-09), the Youth Innovation Promotion Association CAS (Grant No. 2021192), the IMR Innovation Fund (2023-ZD01) and the Joint Research Project between Chinese Academy of Sciences (CAS) (Grants 174321KYSB20210002) and Scientific and Technological Research Council of Turkey (TUBITAK) (No: 121N772).

References

[1] Hu Y, Cheng H, Yu JH. An experimental study on crack closure induced by laser peening in pre-cracked aluminum alloy 2024-T351 and fatigue life extension. Int J Fatig 2020;130:105232.
[2] Qin Z, Li B, Huang X, et al. The effect of laser shock peening on surface integrity and high and very high cycle fatigue properties of 2024-T351 aluminum alloy. Opt Laser Technol 2022;149:107897.
[3] Liu A, Xu ZW, Liang Z, Wang XS. An evaluation on high cycle fatigue fracture characteristics of 2024-T351 Al alloy with different surface defects. Mech Mater 2022;164:104133.
[4] Khan AS, Liu H. A new approach for ductile fracture prediction on Al 2024-T351 alloy. Int J Plast 2012;35:1–12.
[5] Taghizadeh H, Chakherlou TN, Aghdam AB. Prediction of fatigue life in cold expanded Al-alloy 2024-T3 plates used in double shear lap joints. J Mech Sci Technol 2013;27:1415–25.
[6] Chen YQ, Pan SP, Zhou MZ. Effects of inclusions, grain boundaries and grain orientations on the fatigue crack initiation and propagation behavior of 2524-T3 Al alloy. Mater Sci Eng 2013;580:150–8.
[7] Gazizov MR, Kaibyshev RO. Kinetics and fracture behavior under cycle loading of an Al-Cu-Mg-Ag alloy. Phys Met Metallogr 2016;117:725–34.
[8] Gao C, Ma Y, Tang L-z, et al. Microstructural evolution and mechanical behavior of friction spot welded 2198-T8 Al-Li alloy during aging treatment. Mater Des 2017;115:224–30.
[9] Sharma VMJ, Kumar KS, Rao BN. Fatigue crack growth of AA2219 under different aging conditions. Mater Sci Eng 2011;528:4040–9.
[10] Shan ZJ, Liu SD, Ye LY, et al. Mechanism of precipitate microstructure affecting fatigue behavior of 7020 aluminum alloy. Materials 2020;13:3248.
[11] Desmukh MN, Pandey RK, Mukhopadhyay AK. Effect of aging treatments on the kinetics of fatigue crack growth in 7010 aluminum alloy. Mater Sci Eng 2006;435:318–26.
[12] Liu YC, Pan QL, Liu B, et al. Effect of aging treatments on fatigue properties of 6005A aluminum alloy containing Sc. Int J Fatig 2022;163:107103.
[13] Hornbogen E, Gahr KHZ. Microstructure and fatigue crack growth in a γ-Fe-Ni Al Alloy. Acta Metall 1976;24:581–92.
[14] Gong BS, Zhang ZJ, Qu Z, et al. Effect of aging state on fatigue property of wrought aluminum alloys. Int J Fatig 2022;156:106682.
[15] Gong BS, Zhang ZJ, Duan QQ, et al. Effects of aging state on fatigue properties of 6A01 aluminum alloy. Fatig Fract Eng Mater Struct 2022;45:1751–62.
[16] Han WZ, Chen Y, Vinogradov A, et al. Dynamic precipitation during cyclic deformation of an underaged Al-Cu alloy. Mater Sci Eng 2011;528:7410–6.
[17] Horibe S, Laird C. Cyclic stress-strain behavior at a high strain amplitude of Al-Cu crystals containing partially coherent precipitates. Mater Sci Eng 1985;72:149–53.
[18] Pahl RG, Cohen JB. Effects of fatigue on the GP zones in Al-Zn alloys. Metall Mater Trans 1984;15:1519–29.
[19] Souami N, Fagot M, Chomel P, et al. Fatigue particle coarsening in Al-Zn alloy. Scripta Metall 1986;20:1673–6.
[20] Coffin LF. A study of the effects of cyclic thermal stresses on a ductile metal, vol. 76. American Society of Mechanical Engineers; 1954. p. 931–50.
[21] Manson SS. National advisory committee on aerospace technical note 2933. Cleveland, OH: National Advisory Committee; 1954.
[22] Mughrabi H, Höppel HW. Cyclic deformation and fatigue properties of very fine-grained metals and alloys. Int J Fatig 2010;32:1413–27.
[23] Mughrabi H, Höppel HW. Cyclic deformation and fatigue properties of ultrafine grain size materials: current status and some criteria for improvement of the fatigue resistance. Mrs Proceedings 2001;634. B2.1.1-B2.1.12.
[24] Agnew SR, Weertman JR. Cyclic softening of ultra fine grained copper. Mater Sci Eng 1998;244:145–52.
[25] Li P, Li SX, Wang ZG, et al. Fundamental factors on formation mechanism of dislocation arrangements in cyclically deformed fcc single crystals. Prog Mater Sci 2011;56:328–77.
[26] Liu R, Zhang ZJ, Zhang P, et al. Extremely-low-cycle fatigue behaviors of Cu and CuAl alloys: damage mechanisms and life prediction. Acta Mater 2015;83:341–56.
[27] An XH, Wu SD, Wang ZG, et al. Enhanced cyclic deformation responses of ultrafinegrained Cu and nanocrystalline Cu-Al alloys. Acta Mater 2014;74:200–14.
[28] An XH, Liu QY, Wu SD, et al. Improved fatigue strength of nanostructured Cu and Cu-Al alloys. Materials Research Letters 2015;3:135–41.
[29] Shao CW, Zhang P, Liu R, et al. Low-cycle and extremely low cycle fatigue behaviors of high-Mn austenitic TRIP/TWIP alloys: property evaluation, damage mechanisms and life prediction. Acta Mater 2016;103:781–95.
[30] Li Y, Shi ZS, Lin JG. Experimental investigation and modelling of yield strength and work hardening behaviour of artificially aged Al-Cu-Li alloy. Mater Des 2019;183:108121.
[31] Fribourg G, Brechet Y, Deschamps A, et al. Microstructure-based modelling of isotropic and kinematic strain hardening in a precipitation-hardened aluminum alloy. Acta Mater 2011;59:3621–35.
[32] Deschamps A, Decreus B, De Geuser F, et al. The influence of precipitation on plastic deformation of Al-Cu-Li alloys. Acta Mater 2013;61:4010–21.

[33] Teixeira JD, Cram DG, Bourgeois L, et al. On the strengthening response of aluminum alloys containing shear-resistant plateshaped precipitates. Acta Mater 2008;56:6109–22.
[34] Qu Z, Zhang ZJ, Yan JX, et al. Examining the effect of the aging state on strength and plasticity of wrought aluminum alloys. J Mater Sci Technol 2022;122:54–67.
[35] Tayon WA, Nygren KE, Crooks RE, et al. In-situ study of planar slip in a commercial aluminum-lithium alloy using high energy X-ray diffraction microscopy. Acta Mater 2019;173:231–41.
[36] Gerold V, Karnthaler HP. On the origin of planar slip in f.c.c. alloys. Acta Metall 1989;37:2177–83.
[37] Hirsch PB, Humphreys F. The deformation of single crystals of copper and copper-zinc alloys containing alumina particles-I. Macroscopic properties and workhardening theory. Proceedings of the Royal Society 1970;318:45–72.
[38] Wang SC, Starink MJ. Precipitates and intermetallic phases in precipitation hardening Al-Cu-Mg-(Li) based alloys. Int Mater Rev 2005;50:193–215.
[39] Hutchinson CR, Ringer SP. Precipitation processes in Al-Cu-Mg alloys microalloyed with Si. Metall Mater Trans 2000;31:2721–33.
[40] Alexopoulos ND, Velonaki Z, Stergiou CI, et al. The effect of artificial ageing heat treatments on the corrosion-induced hydrogen embrittlement of 2024 (Al-Cu) aluminum alloy. Corrosion Sci 2016;102:413–24.
[41] da Costa Teixeira J, Bourgeois L, Sinclair CW, et al. The effect of shear-resistant, plate-shaped precipitates on the work hardening of Al alloys: towards a prediction of the strength-elongation correlation. Acta Mater 2009;57:6075–89.
[42] Srivatsan TS. The low-cycle fatigue and cyclic fracture behavior of 7150 aluminum alloy. Int J Fatig 1991;4:313–21.
[43] Song MS, Kong YY, Ran MW, et al. Cyclic stress-strain behavior and low cycle fatigue life of cast A356 alloys. Int J Fatig 2011;33:1600–7.
[44] Sekhar AP, Nandy S, Bakkar MA, et al. Low cycle fatigue response of differently aged AA6063 alloy: statistical analysis and microstructural evolution. Materialia 2021;20:101219.
[45] Basquin OH. The exponential law of endurance tests. American Society for Testing and Materials 1910;10:625–30.
[46] Manson SS. Fatigue: a complex subject-Some simple approximations. Exp Mech 1965;5:193–226.
[47] Meggiolaro MA, Castro JTP. Statistical evaluation of strain-life fatigue crack initiation predictions. Int J Fatig 2004;26:463–76.